sustainability

MDPI

Article

Target Selection for a Space-Energy Driven Laser-Ablation Debris Removal System Based on Ant Colony Optimization

Wulin Yang [1,2], Hongya Fu [1], Zhongxi Shao [1,*], Qiang Wu [2] and Chuan Chen [2]

[1] School of Mechatronics Engineering, Harbin Institute of Technology, Harbin 150001, China; 18B908031@stu.hit.edu.cn (W.Y.); hongyafu@hit.edu.cn (H.F.)
[2] Beijing Institute of Spacecraft Environment Engineering, Beijing 100091, China; wuqiang12525@126.com (Q.W.); chenchuan0611@163.com (C.C.)
* Correspondence: shaozhongxi78@163.com

Abstract: The space-energy driven laser-ablation debris removal technology can remove or detach multiple centimeter-level space debris in a single mission. However, the space-energy driven platform can only rely on its own equipment capabilities to detect and identify space debris. It is necessary to select multiple potentially removable debris targets to improve the removal efficiency. In this paper, target selection for a space-energy driven laser-ablation debris removal system is analyzed based on ant colony optimization. The intersection and interaction periods were given by the optimal driving sequence calculation for multiple debris. Parameters such as the detection range, pulsed energy, repetition frequency of the laser and trajectory of debris have been considered as inputs of the simulation. Target selection and optimal action time have been calculated when a single debris entered the detection range of the laser system. This optimization can significantly improve the overall efficiency and laser energy utilization of the space-based laser platform for the same randomly generated debris group, compared to the mode driven sequentially according to the order of entering the laser action range. The results showed that after being filtered by the ant colony algorithm, the number of removable debris doubled, and the de-orbit altitude increased by 15.9%. The energy utilization rate of the laser removal system has been improved by 74.6%. This optimization algorithm can significantly improve the overall work efficiency and laser energy utilization rate of the space-energy driven system. It can remove more debris or have a larger effective orbit reduction distance value for all debris.

Keywords: space-energy; laser ablation; space-based laser; target selection; ant colony optimization

check for updates

Citation: Yang, W.; Fu, H.; Shao, Z.; Wu, Q.; Chen, C. Target Selection for a Space-Energy Driven Laser-Ablation Debris Removal System Based on Ant Colony Optimization. *Sustainability* **2023**, *15*, 10380. https://doi.org/10.3390/su151310380

Academic Editor: Maxim A. Dulebenets

Received: 10 May 2023
Revised: 27 June 2023
Accepted: 27 June 2023
Published: 30 June 2023

Copyright: © 2023 by the authors. Licensee MDPI, Basel, Switzerland. This article is an open access article distributed under the terms and conditions of the Creative Commons Attribution (CC BY) license (https://creativecommons.org/licenses/by/4.0/).

1. Introduction

Space debris is a non-functional artificial object and its components operate in orbit or re-enter the atmosphere on Earth. With the increasing frequency of space activities, the amount of space debris has rapidly increased, posing a great threat to the safe operation of in-orbit assets and the conduct of space activities [1]. The international community has continued to pay attention to this issue, and countries around the world have reached a broad consensus on jointly carrying out space debris environmental governance [2]. The measures taken for post-mission disposal and collision avoidance of space debris are insufficient to suppress the continuous deterioration of the space debris environment. The current international consensus is that the active removal of space debris is an inevitable choice and the only way to ensure the long-term sustainability of space [3–5].

Currently, most active space debris removal technologies, including robotic arm capture, fly net capture, harpoons, etc., are mainly aimed at large-sized debris above the meter level and are difficult to apply to the removal of space debris on a scale of 1–10 cm [6–8]. However, there is an urgent need to remove debris on a scale of 1–10 cm. On the one hand, 1–10 cm debris cannot be actively avoided or passively protected at the current technological level,

which is the main factor causing fatal damage to spacecrafts [9–11]. Targeted active removal is needed to ensure the safety of spacecraft in orbit. On the other hand, due to the large amount and the frequent collisions with each other, debris can generate secondary debris when they collide [12–14]. It is necessary to actively remove them to suppress the continuous deterioration of the space debris environment.

Space-energy driven laser-ablation debris removal involves using a strong laser beam to irradiate the surface of the debris, causing the melting, vaporization, and ionization of the material in the irradiation zone and forming of a plasma plume [15,16]. The impulse coupling of the plasma plume causes the debris to obtain a reverse velocity increment, thereby driving the movement of the debris, changing its orbit, and lowering it into the atmosphere to achieve removal. This technology has the characteristics of simple operation, long action distance, rapid response, low cost, and high reliability [17]. It is especially suitable for the removal of 1–10 cm scale debris.

Due to the difficulty in tracking and cataloging 1–10 cm debris, the potential target cannot be predicted and must be detected independently by the laser platform [18]. It is hard to develop removal strategies in advance like the mechanical capture debris removal method. During the removal period, the laser platform may discover multiple space debris at the same time. Each of the detected debris may enter the ablation range, with a limited time window and potential conflicts [19]. It is necessary to analyze, select and plan tasks in real-time based on the detected debris.

The optimization of the selection and removal sequence of multiple debris during laser removal is essentially the path optimization of the removal system. There are many mature algorithms for path optimization. Ant colony optimization algorithms have good robustness and excellent global search ability, which can quickly achieve the global optimization [20–22].The core idea of ant colony optimization is the self-organizing collective behavior of ants during foraging. It means that the shortest distance between the food source and the nest can be found through collective search behavior. When ants move between the food source and the nest, they will release a volatile pheromone along the way, and other ants will follow the path of the released pheromone, and eventually the ants can converge to the same path. At present, the max/min ant colony optimization can avoid premature convergence and achieve better performance, making it the best ant colony optimization algorithm to solve problems such as the traveling salesman and quadratic allocation [23].

In this paper, mission planning based on the typical task flow of space-based laser driven space debris removal is introduced. Single and multi debris de-orbit optimization control algorithms were established based on the ant colony algorithm. The computational effectiveness was verified using the debris generated near the platform orbit based on the platform orbit information as an input.

2. Target Selection Model

Due to the requirement of tracking accuracy, space-based laser platforms cannot perform laser irradiation under the guidance of other platforms. Even with the support of additional detection data, the laser ablation process still needs to rely on the platform's own tracking and aiming equipment to detect and capture the target. When debris is detected, it is necessary to determine whether it will enter the platform's range of action based on its trajectory, in order for the debris to be ablated. During the ablation process, the impulse determines whether the interaction can effectively lower the orbit or propel the debris away. The impulse direction generated by laser ablation is determined by the relative positions of the debris and laser platform. Debris that enters the scope of ablation has a limited time window, during which effective trajectory changes can be achieved through propulsion. The process is illustrated in Figure 1. When multiple debris enter the scope of action simultaneously or sequentially, challenges arise regarding the order of ablation and selection in the presence of time conflicts. This requires further optimization of the optimal action sequence based on their respective time windows and expected driving effects.

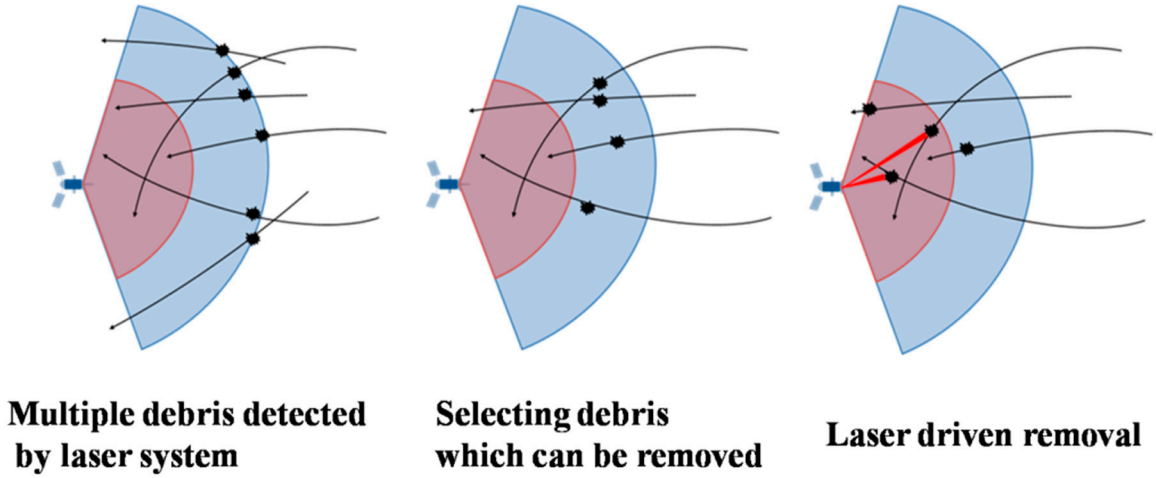

Figure 1. Typical task flow for removing debris on a space-based laser platform.

Based on the introduction above, the process of a space-energy driven laser-ablation debris removal system is as follows:

1. n targets T_1-T_n were found at time t_0-t_1.
2. Calculate and filter the discovered debris to eliminate those that do not fall within the scope of the platform.
3. Single target selection optimization. Calculate the relative position change of all targets that will enter the scope of action one by one according to their estimated tracks. Analyze their optimal action time when they can be effectively cleared (perigee is less than 200 km) to obtain the optimal driving time.
4. Multi objective sequence optimization. With the goal of achieving the best overall driving effect throughout the entire time period, analyze the time conflict situation of the action window for all targets entering the range of action, resolve conflicts, and form a driving time sequence.
5. After the target enters the range, it is sequentially driven according to the sequence.

2.1. Centimeter Space Debris Removal Scene

Due to the lack of a cataloging database for centimeter-level space debris, it is necessary to construct a simulation calculation scenario that is as close to the actual situation as possible based on the centimeter-level space debris data near the laser platform orbit. The generated debris is the calculation input for sequence optimization. In this article, based on the orbital parameters of the debris removal platform, the Monte Carlo random sampling method is used to construct the orbital elements of the initial space debris near the production platform orbit in Equations (1) and (2) [24].

$$\begin{aligned} \vec{R}_m &= \vec{R}_{sc} + d\vec{R}_m \\ &= \vec{R}_{sc} + dR_m \begin{bmatrix} \cos Ele \cos Az \\ \cos Ele \sin Az \\ \sin Ele \end{bmatrix} \end{aligned} \tag{1}$$

$$\vec{V}_m = V_m \begin{bmatrix} \cos\alpha \sin\beta \\ \cos\alpha \cos\beta \\ \sin\alpha \end{bmatrix} \tag{2}$$

A_z is the azimuth angle of the debris relative to the removal system, Ele is the elevation angle of the debris relative to the removal system, dR_m is the relative position vector of

debris m relative to the laser platform in the inertial frame, where dR_m meets the detection distance requirement [25]. V_m is the velocity vector of debris m in the inertial frame, where

$$V_m \in \left[\sqrt{\frac{\mu}{R_{\max}}}, \sqrt{\frac{\mu}{R_{\min}}}\right] \tag{3}$$

Based on Equation (3), the initial space debris dataset can be obtained by using the Monte Carlo random sampling method. It can be sorted according to the distribution characteristics of space debris; for example, the orbital inclination of debris is less than 100° and the eccentricity is less than 0.05. If the perigee of debris is greater than 200 km, the space debris database can be obtained.

The coordinate transformation matrix from the inertial coordinate system to the orbital coordinate system (RSW) is in Equation (4) [26]:

$$\begin{gathered} R_{oi} = R_z(u)R_x(i)R_z(\Omega) \\ = \begin{bmatrix} \cos u\cos\Omega - \sin u\cos i\sin\Omega & \cos u\sin\Omega + \sin u\cos i\cos\Omega & \sin u\sin i \\ -\sin u\cos\Omega - \cos u\cos i\sin\Omega & -\sin u\sin\Omega + \cos u\cos i\cos\Omega & \cos u\sin i \\ \sin i\sin\Omega & -\sin i\cos\Omega & \cos i \end{bmatrix} \\ \begin{bmatrix} x_i \\ y_i \\ z_i \end{bmatrix} = R_{io}\begin{bmatrix} r \\ 0 \\ 0 \end{bmatrix} = \frac{a(1-e^2)}{1+e\cos f}\begin{bmatrix} \cos u\cos\Omega - \sin u\cos i\sin\Omega \\ \cos u\sin\Omega + \sin u\cos i\cos\Omega \\ \sin u\sin i \end{bmatrix} = r\begin{bmatrix} \cos\delta\cos\alpha \\ \cos\delta\sin\alpha \\ \sin\delta \end{bmatrix} \end{gathered} \tag{4}$$

δ and α are the declination and right ascension of the debris, respectively. If the positions of two space debris are equivalent, it is obvious in Equation (5) that:

$$\begin{gathered} \frac{a_s(1-{e_s}^2)}{1+e_s\cos f_s} = \frac{a(1-e^2)}{1+e\cos f} \\ \begin{bmatrix} \cos u_s\cos\Omega_s - \sin u_s\cos i_s\sin\Omega_s \\ \cos u_s\sin\Omega_s + \sin u_s\cos i_s\cos\Omega_s \\ \sin u_s\sin i_s \end{bmatrix} = \begin{bmatrix} \cos u\cos\Omega - \sin u\cos i\sin\Omega \\ \cos u\sin\Omega + \sin u\cos i\cos\Omega \\ \sin u\sin i \end{bmatrix} \end{gathered} \tag{5}$$

If the initial position of the laser platform is near the ascending/descending intersection point, Monte Carlo random sampling results in a probability of generating debris that meet the requirements of around 4%. If there is a chance of a close intersection for two space debris with different orbital inclinations, the time window of the leap is near to the ascending or descending intersection point. According to Formula (3), it is necessary to meet the following conditions in Equation (6) [27]:

$$\begin{gathered} \frac{a_s(1-{e_s}^2)}{1+e_s\cos f_s} = \frac{a(1-e^2)}{1+e\cos f} \\ \begin{bmatrix} \cos u_s\cos\Omega_s - \sin u_s\cos i_s\sin\Omega_s \\ \cos u_s\sin\Omega_s + \sin u_s\cos i_s\cos\Omega_s \\ \sin u_s\sin i_s \end{bmatrix} = \begin{bmatrix} \cos\Omega \\ \sin\Omega \\ 0 \end{bmatrix} \end{gathered} \tag{6}$$

2.2. Single Debris Selection

The single debris optimization control algorithm needs to target single space debris. Based on the input of space debris, laser system and optimal de-orbit effect, the laser ablation sequence can be determined. The laser ablation sequence includes start point, end point, total period of the ablation and total pulse number of the laser system. The optimal sequence is the shortest working time of the laser when two sequences can achieve the same de-orbit reduction effect.

2.2.1. Laser Impulse Calculation

According to the information of the space debris and laser system, the maximum de-orbit effect of debris can be calculated. If the perigee of space debris is lower than 200 km, it will be seen as successful removal.

Simplify space debris as a planar target for laser impulse calculation, with the following formula in Equation (7) [28]:

$$f_L \tau_L' = \frac{\boldsymbol{I}_0}{m} = \frac{C_m I_L \tau_L A_L}{m} \cos(\hat{\boldsymbol{n}}, \hat{\boldsymbol{L}}_R)\hat{\boldsymbol{n}} \tag{7}$$

where C_m is the impulse coupling coefficient, I_L is the laser power density, τ_L is the laser pulse width, A_L is the laser irradiation area, $\hat{n}$ is the normal vector irradiated by a laser, $\hat{L}_R$ is the direction of laser irradiation. The conditions for the target material to be irradiated by the laser are in Equation (8):

$$\cos(\hat{\boldsymbol{n}}, \hat{\boldsymbol{L}}_R) < 0 \tag{8}$$

In this study, it is assumed that the space debris is a circular aluminum alloy thin plate. The plane normal vector irradiated by the laser is in the opposite direction to the laser irradiation direction. We make this assumption because in current detection methods it is difficult to obtain centimeter-level debris dimensions and material information at a long distance.

2.2.2. Orbital Motion Model

Based on the relative motion between the space debris and laser platform, the intersection process between debris and the platform can be obtained. For space debris (perigee below 400 km), the long-term impact of atmospheric drag on orbit must be considered, and the formula for calculating atmospheric drag is in Equation (9) [29]:

$$\begin{array}{l} \boldsymbol{f}_D = -\frac{C_D A}{2m} \rho V \boldsymbol{V} \\ \boldsymbol{V} = \boldsymbol{v} - \boldsymbol{\omega}_e \times \boldsymbol{r} \end{array} \tag{9}$$

where $C_D \approx 2.2$ is the resistance coefficient, A/m is the surface to mass ratio of space debris, ω_e is the rotational velocity of the Earth. According to the fitting formula of American standard atmosphere model, the atmospheric density of 200–600 km can be calculated by the formula below in Equation (10):

$$\begin{array}{l} \ln(\frac{\rho}{\rho_m}) = -9.595 - 9.7875 \times 10^{-3}(\frac{h}{h_u} - 200) + \\ 7.0725 \times 10^{-6}(\frac{h}{h_u} - 200)(\frac{h}{h_u} - 400) \end{array} \tag{10}$$

Under the combined action of laser ablation force and atmospheric resistance, the movement of space debris can be described by position velocity in Equation (11) [30]:

$$\begin{array}{ll} \ddot{\vec{\boldsymbol{r}}}_s & = \boldsymbol{g}(\vec{\boldsymbol{r}}_s) + \boldsymbol{f}_{D,s} \\ \ddot{\vec{\boldsymbol{r}}}_d & = \boldsymbol{g}(\vec{\boldsymbol{r}}_d) + \boldsymbol{f}_{D,d} + \boldsymbol{f}_L(\vec{\boldsymbol{r}}_d, \vec{\boldsymbol{r}}_s) \\ & = \boldsymbol{g}(\vec{\boldsymbol{r}}_d) + \boldsymbol{f}_{D,d} + F_{\max} u \cdot \vec{\boldsymbol{n}} \end{array} \tag{11}$$

Compared with the average laser ablation force, the impact of atmospheric drag can be ignored in sequence planning when the altitude of the space debris is higher than 400 km. At this point, the equation can be expressed as in Equations (12)–(14) [31]:

$$\begin{cases} \dot{\vec{\boldsymbol{r}}}_s = \vec{\boldsymbol{v}}_s \\ \dot{\vec{\boldsymbol{v}}}_s = -\mu \frac{\vec{\boldsymbol{r}}_s}{r_s^3} \\ \dot{\vec{\boldsymbol{r}}}_d = \vec{\boldsymbol{v}}_d \\ \dot{\vec{\boldsymbol{v}}}_d = -\mu \frac{\vec{\boldsymbol{r}}_d}{r_d^3} + F_{\max} u \cdot \vec{\boldsymbol{n}} \end{cases} \tag{12}$$

$$F_{\max} = \begin{cases} 0 & if \| \vec{\boldsymbol{r}}_d - \vec{\boldsymbol{r}}_s \| > r_{\min} \\ C_m E f_L / M & else \end{cases} \tag{13}$$

$$\vec{\boldsymbol{n}} = \frac{\vec{\boldsymbol{r}}_d - \vec{\boldsymbol{r}}_s}{\| \vec{\boldsymbol{r}}_d - \vec{\boldsymbol{r}}_s \|} \tag{14}$$

where $u \in [0, 1]$ is the on/off condition of the laser system.

Under the $\sigma(t) = h_{p,\min} - \phi(t) = h_{p,\min} - h_p(\boldsymbol{r}_d, \boldsymbol{v}_d) \leq 0$ condition, an appropriate optimal control rate to minimize the debris perigee, or minimize the startup time when the perigee height is less than 200 km can be given. The minimum performance index function can be described as in Equations (15) and (16) [32]:

$$\begin{aligned} J &= h_p(t_f) + \lambda_0 \int_{t_0}^{t_f} u F_{\max} \mathrm{d}t \\ &= [a(1-e) - R_E] + \int_{t_0}^{t_f} \lambda_0 u F_{\max} \mathrm{d}t \\ &= \phi\left(\vec{\boldsymbol{r}}_d(t_f), \vec{\boldsymbol{v}}_d(t_f)\right) + \int_{t_0}^{t_f} L\left(\vec{\boldsymbol{r}}_d, \vec{\boldsymbol{v}}_d, u F_{\max}\right) \mathrm{d}t \end{aligned} \tag{15}$$

where

$$a = \left(\frac{2}{r_d(t_f)} - \frac{v_d(t_f)^2}{\mu} \right)^{-1}, e = \sqrt{\left[1 - \frac{r_d(t_f)}{a}\right]^2 + \frac{r_d(t_f)^2 v_d(t_f)^2}{\mu a}} \tag{16}$$

This is a typical optimal control problem with state space constraints. When solving based on the indirect method in optimal control, the Lagrangian function is in Equations (17) and (18) [33]:

$$J_\alpha = J + \int_{t_0}^{t_f} \kappa \cdot \sigma \mathrm{d}t = \phi + \int_{t_0}^{t_f} (L + \kappa \cdot \sigma) \mathrm{d}t \tag{17}$$

$$\psi = H + \kappa \cdot \sigma = L + \lambda \cdot \dot{\boldsymbol{x}} + \kappa \cdot \sigma \tag{18}$$

The Hamiltonian function is in Equation (19):

$$\begin{aligned} H &= \vec{\boldsymbol{\lambda}} \cdot \dot{\vec{\boldsymbol{x}}} + L(\boldsymbol{x}, u, t) \\ &= \vec{\boldsymbol{\lambda}}_r \cdot \vec{\boldsymbol{v}}_d + \vec{\boldsymbol{\lambda}}_v \cdot (-\mu \frac{\vec{\boldsymbol{r}}_d}{r_d^3} + F_{\max} u \cdot \vec{\boldsymbol{n}}) + \lambda_0 u F_{\max} \\ &= \vec{\boldsymbol{\lambda}}_r \cdot \vec{\boldsymbol{v}}_d - \vec{\boldsymbol{\lambda}}_v \cdot (\mu \frac{\vec{\boldsymbol{r}}_d}{r_d^3}) + (\lambda_0 + \vec{\boldsymbol{\lambda}}_v \cdot \vec{\boldsymbol{n}}) F_{\max} u \\ \dot{\vec{\boldsymbol{\lambda}}} &= -\frac{\partial H}{\partial \boldsymbol{x}} - \kappa \frac{\partial \sigma}{\partial \boldsymbol{x}} \\ \dot{\vec{\boldsymbol{\lambda}}}_r &= \frac{\mu}{r_d^3} \left(\vec{\boldsymbol{\lambda}}_v - \frac{3(\vec{\boldsymbol{\lambda}}_v \cdot \vec{\boldsymbol{r}}_d)}{r_d^2} \vec{\boldsymbol{r}}_d \right) - \kappa \frac{\partial \sigma}{\partial \vec{\boldsymbol{r}}_d} \\ &= \frac{\mu}{r_d^3} \left(\vec{\boldsymbol{\lambda}}_v - \frac{3(\vec{\boldsymbol{\lambda}}_v \cdot \vec{\boldsymbol{r}}_d)}{r_d^2} \vec{\boldsymbol{r}}_d \right) + \kappa \frac{\partial \phi}{\partial \vec{\boldsymbol{r}}_d} \\ \dot{\vec{\boldsymbol{\lambda}}}_v &= -\vec{\boldsymbol{\lambda}}_r - \kappa \frac{\partial \sigma}{\partial \vec{\boldsymbol{v}}_d} \\ &= -\vec{\boldsymbol{\lambda}}_r + \kappa \frac{\partial \phi}{\partial \vec{\boldsymbol{v}}_d} \end{aligned} \tag{19}$$

λ_0 is the weight coefficient of perigee height and laser power on time.

According to the optimal control rate, the Hamilton function can be minimized as follows. When u is a continuous function in Equation (20),

$$\frac{\partial H}{\partial u} = 0 \tag{20}$$

when u is discontinuous in Equation (21),

$$u_* = \arg_{u\in[0,1]} \min H \tag{21}$$

That means $u = 1, \quad if(\rho < 0)$, the switch function is $\rho = (\lambda_0 + \vec{\lambda}_v \cdot \vec{n})F_{\max}$, $\vec{n} = \frac{\vec{r}_d - \vec{r}_s}{\|\vec{r}_d - \vec{r}_s\|}$. At the same time, the relaxation conditions $\kappa \cdot \sigma = 0, \quad \kappa \geq 0, \sigma \leq 0$ are met. This indicates that the clearance height constraint $\sigma = 0$ is reached, the perigee will not change and no force $u = 0$ will be applied. Otherwise,$\kappa = 0$. At the same time, the terminal covariate variables need to meet Equation (22):

$$\begin{cases} \vec{\lambda}_r(t_f) = \frac{\partial \phi}{\partial \vec{r}_d(t_f)} \\ \vec{\lambda}_v(t_f) = \frac{\partial \phi}{\partial \vec{v}_d(t_f)} \end{cases} \tag{22}$$

The solution is divided into two steps. First, solve the optimal control problem of the lowest perigee altitude $\kappa = 0$ to obtain the time window for orbit descent. For space debris that can be cleared, the laser on/off time is optimized to minimize the laser working period.

2.3. Multiple Debris Selection

To solve the combinatorial optimization problem, expressing it in a standard format is the first step. Then, use the ant colony algorithm to determine the decision point according to the pheromone as the feedback carrier between exploration and utilization. Construct the pheromone of each ant individual incrementally according to the corresponding pheromone-updated rules. Plan the behavior direction of the ant colony activity from the overall perspective. Work out the optimal solution of the combinatorial optimization problem from the cycle. The process is shown in Figure 2.

The continuous ant colony algorithm (CACA) is a method that extends traditional ant colony algorithms to continuous domains. Theoretically, the global optimal obtained through this algorithm. Due to its proximity to the original formula of ant colony algorithm, ACOR has the potential to solve mixed discrete–continuous optimization problems [34]. But, this article mainly studies its use to solve pure continuous optimization problems.

The core idea of ant colony algorithms is to select solutions based on a biased probability and gradually build a complete solution set. In each step, ants choose the composition of the solution from the feasible solution by the probability property according to the formula in Equation (23) [35]:

$$\begin{aligned} p(c_{ij}|s^p) &= \frac{{\tau_{ij}}^{\alpha} \cdot \eta(c_{ij})^{\beta}}{\sum\limits_{c_{il}\in N(s^p)} {\tau_{il}}^{\alpha} \cdot \eta(c_{il})^{\beta}}, \forall c_{ij} \in N(s^p) \\ P_i(j) &= \sum_{c_{il}\in N(s^p)} {\tau_{il}}^{\alpha} \cdot \eta(c_{il})^{\beta} \end{aligned} \tag{23}$$

Each element of the feasible solution and its probability constitute the discrete probability distribution of the ant sampling, so as to select the elements to be added to the current solution space C_{ij} is the j-th element of the solution constructed by ant i, which is

heuristic information and is generally chosen as the reciprocal of the objective function. The pheromone τ_{ij} is updated as follows in Equation (24) [36]:

$$\tau_{ij} = \begin{cases} (1-\rho)\tau_{ij} + \rho\Delta\tau & \text{if} \quad \tau_{ij} \in s_{ch} \\ (1-\rho)\tau_{ij} & \text{otherwise} \end{cases} \tag{24}$$

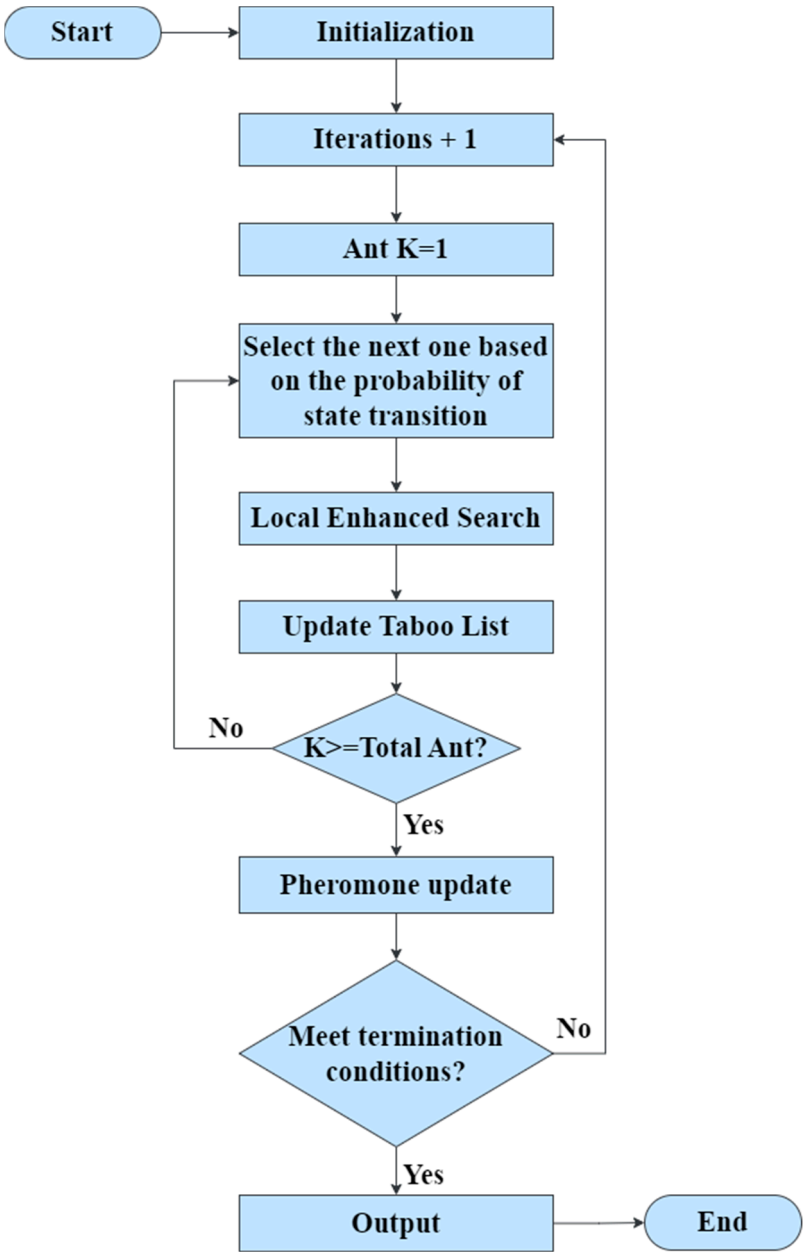

Figure 2. Flowchart of basic ant colony algorithm.

Pheromone Q/L_k is usually updated with global information $\Delta\tau$, which has a good performance in solving TSP problems.

Referring to the idea of discrete probability distribution in the ant colony algorithm, ACOR proposes a continuous probability distribution for variable optimization in a contin-

uous domain. It is further transformed into sampling in the Gaussian kernel probability density function G^I in Equation (25) [37]:

$$\begin{aligned} G^i(x) &= \sum_{l=1}^{k} \omega_l g_l^i(x) = \sum_{l=1}^{k} \omega_l \frac{1}{\sigma_l^i} e^{-\frac{(x-\mu_l^i)^2}{2\sigma_l^{i2}}} \\ \mu_l^i &= s_l^i \\ \omega_l &= \frac{1}{qk\sqrt{2\pi}} e^{-\frac{(l-1)^2}{2q^2k^2}} \\ \sigma_l^i &= \xi \sum_{e=1}^{k} \frac{|s_e^i - s_l^i|}{k-1} \end{aligned} \tag{25}$$

where k is the number of stored solutions (which cannot be less than the number of variables), q and ξ are the setting parameters of the algorithm.

The multi debris optimization algorithm needs to calculate the intersection process between debris and the laser system. Time to enter the ablation range, time to leave, time of the intersection window and global de-orbit effect all have to be considered as the optimization goal. The core issue is to resolve conflicts between space debris with conflicting time windows based on single space debris optimization. During the process, it is necessary to consider the rotation time of the laser system attitude. There should be a sufficient time interval between adjacent space debris based on their different positions.

Tabu lists provide important information when making choices in ant colony algorithms [38]. They can be used to solve conflict resolution. In order to achieve decoupling of sequence optimization and on-off time optimization for better optimization efficiency, it is necessary to determine whether the time series between adjacent space debris conflict. The resolution strategy needs to be deterministic to ensure that the sequence and the on/off time can be determined.

The time series relationships between adjacent debris can be divided into four types.

1. $stop_{i-1} + Tse_i \leq bse_i$, if there is no conflict, debris i should be added to the feasible solution.
2. $bse_{i-1} < bse_i - Tse_i < stop_{i-1}$, while $stop_i - Tse_i \geq bse_i - Tse_i \geq stop_{i-1}$, a conflict resolution algorithm needs to be used.
3. $bse_i - Tse_i < bse_{i-1} (< stop_{i-1})$ *and* $stop_{i-1} < stop_i - Tse_i$, some conflicts require the use of conflict resolution algorithms.
4. $bse_i - Tse_i < bse_{i-1}$ *and* $stop_{i-1} \geq stop_i - Tse_i$, if there is a complete conflict and no solution, then debris i should be added to the tabu table.

Among them, numerical integration is required to calculate the benefits $gain_i = f(bse_i, stop_i)$. Steering time $Tse_i = g(stop_{i-1}, arr_i)$ is required to be calculated according to the inertial pointing of the two debris and the attitude response speed of the laser system, which needs to meet the following requirements in Equation (26):

$$\begin{aligned} wait_i &= \mathrm{bse}_i - arr_i \\ &= \mathrm{bse}_i - (stop_{i-1} + Tse_i) \\ &= \mathrm{bse}_i - stop_{i-1} - g(stop_{i-1}, \mathrm{bse}_i) \geq 0 \end{aligned} \tag{26}$$

At the initial stage $wait_i < 0$, it is necessary to adjust bse_i (Strategy 1) or $stop_{i-1}$ (Strategy 2) to meet $Tse_i = g(stop_{i-1}, bse_i) = bse_i - stop_{i-1}$. An iterative algorithm is used to solve the problem. Among them, the strategy selection adopts a greedy strategy. When the profit of the current debris is more than that of the adjustment, the constraint is satisfied, so select strategy 1. Otherwise, choose strategy 2.

When selecting the next debris according to the state transition probability, this paper comprehensively considers decision factors such as pheromone concentration, debris

removal income, removal window length, and waiting time. The calculation formula is as follows in Equation (27) [3]:

$$\begin{aligned} p(c_{ij}|s^p) &= \frac{{\tau_{ij}}^{\alpha} \cdot gain(c_{ij})^{\beta} \cdot [1/width(c_{ij})]^{\gamma} \cdot [1/wait(c_{ij})]^{\delta}}{\sum\limits_{c_{il} \in N(s^p)} {\tau_{il}}^{\alpha} \cdot gain(c_{il})^{\beta} \cdot [1/width(c_{il})]^{\gamma} \cdot [1/wait(c_{il})]^{\delta}}, \forall c_{ij} \in N(s^p) \\ P_i(j) &= \sum_{c_{il} \in N(s^p)} {\tau_{il}}^{\alpha} \cdot gain(c_{il})^{\beta} \cdot [1/width(c_{il})]^{\gamma} \cdot [1/wait(c_{il})]^{\delta} \end{aligned} \quad (27)$$

where $\alpha, \beta, \gamma, \delta$ are the weights of various decision-making factors.

3. Results and Discussion

3.1. Debris Removal Scenarios

The inputs of the simulation are in Table 1. The debris are simplified into circular aluminum alloy sheets with a diameter of 10 cm and a thickness of 1 mm.

Table 1. Laser system configurations.

Parameters Name	Value
Altitude	650 km
Inclination	97.7°
Right ascension	120°
Detection range	200 km
Laser driving range	100 km
Attitude pointing turning speed	$15^{\circ} \cdot s^{-1}$
Laser single pulse energy	300 J
Spot diameter	15 cm
Pulse width	50 nm
Repetition frequency	100 Hz

There are 20,000 debris generated that can enter the detection range of the platform using the laser system orbit as the input. The distribution of these debris is shown in Figures 3 and 4. After target selection, 118 debris can enter the range of the laser system and have a time window for de-orbit.

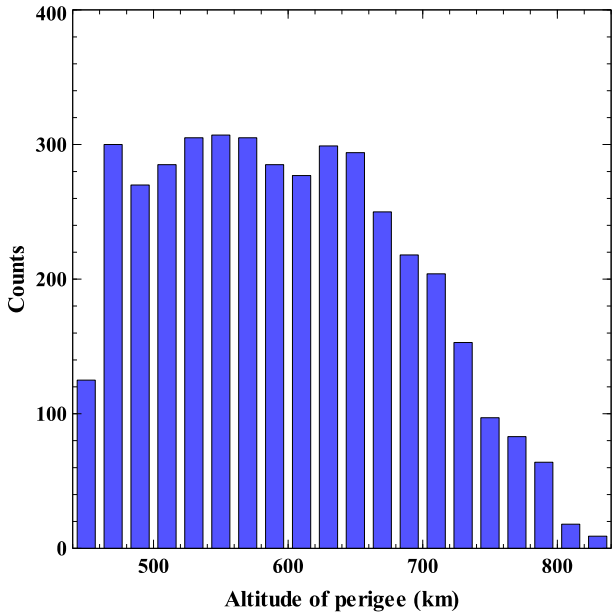

Figure 3. Perigee distribution of space debris.

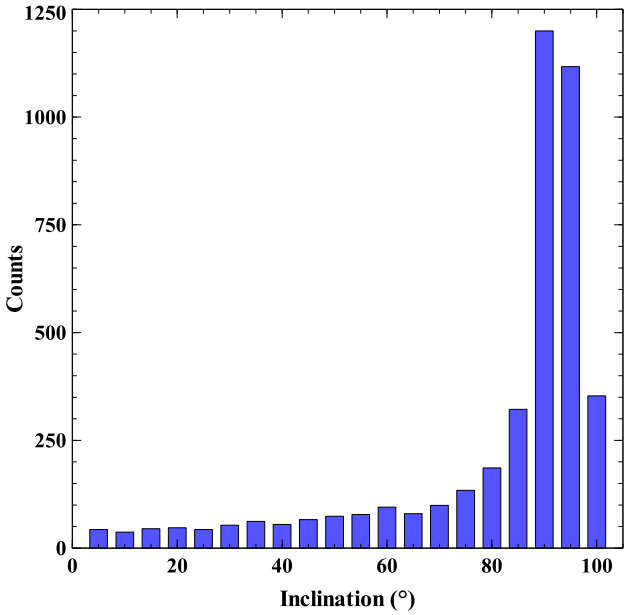

Figure 4. Inclination distribution of space debris.

The distribution of the relative distance and velocity between the space debris and the laser system are shown in Figures 5 and 6. The results showed that the relative velocity between most of the space debris and the laser system is large, making it difficult to remove.

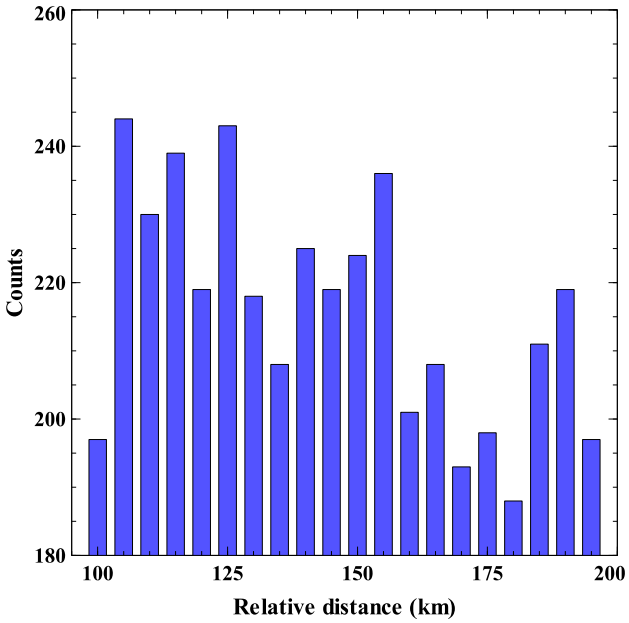

Figure 5. Relative distance distribution between space debris and laser platform.

The results indicated that the intersection of space debris is approximately in the same orbit as the laser system. The orbital inclination and the right ascension of the ascending node are approximately the same. The relative speed is low and the window of time to meet the operating distance is long. Debris can be successfully cleared after a period of laser ablation, but the number of such debris is relatively small. Most of the debris and the laser system have different orbits, with a difference of about 180° in right ascension at the ascending node as shown in Figures 7 and 8. This results in a relatively high relative velocity and a shorter window of time to meet the operating distance, making it difficult to clear.

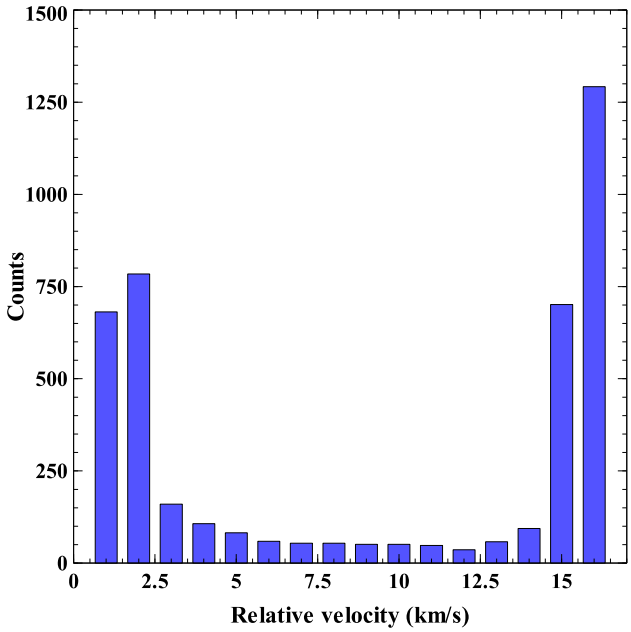

Figure 6. Relative velocity distribution between space debris and laser platform.

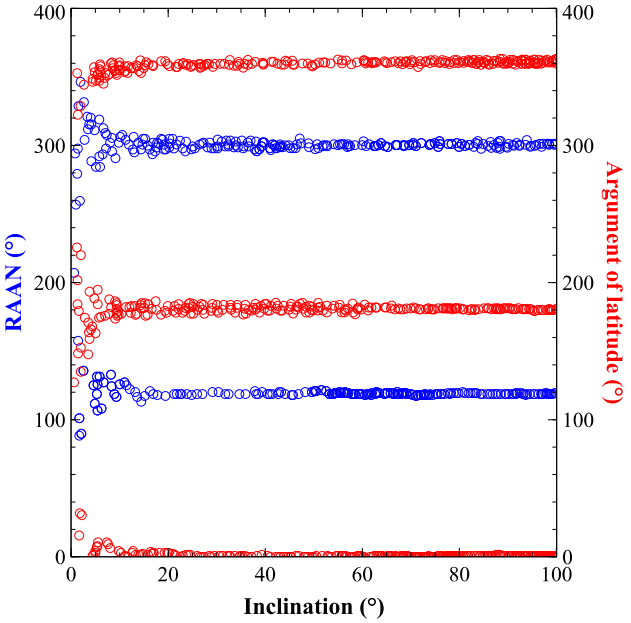

Figure 7. Distribution of declination/latitude argument and orbital inclination of right ascension of the ascending node.

If the initial position of the platform is not near to the ascending/descending intersection point, Monte Carlo random sampling results in the probability of generating debris that meet the requirements of about 1%.

Taking the initial latitude angle of the laser system $u = 120°$, the distribution of debris data is shown in Figures 9 and 10. It is evident that when space debris and the laser system are coplanar, the relative velocity is low. In most cases, space debris and the laser system are not coplanar and have relatively high velocities. At this point,$\sin u_s \sin i_s = \sin u \sin i$ and $\arcsin(\sin u \sin i) \leq i_s, u_s \leq 180° - \arcsin(\sin u \sin i)$.

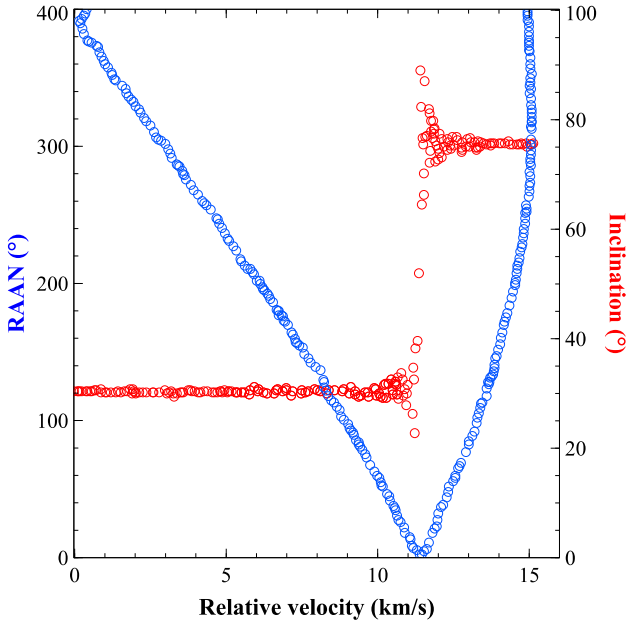

Figure 8. Distribution of relative speed and declination/latitude argument of right ascension of the ascending node.

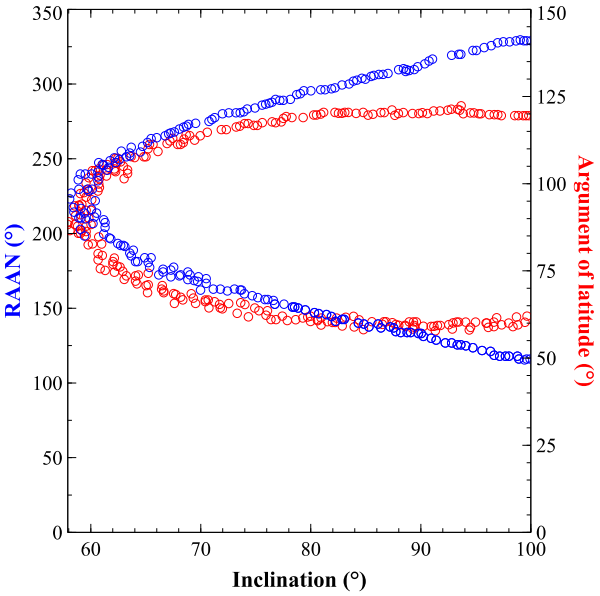

Figure 9. Distribution of inclination and argument of latitude/right ascension of the ascending node.

Taking the initial latitude angle of the laser platform $u = 90°$, the distribution of space debris is shown in Figures 11 and 12. Similar to the previous example, in most cases, the relative speed is relatively high.

3.2. Single Debris selection

For debris with a descent window that cannot be cleared, the descent window is the on-off time corresponding to the maximum change in the height of the debris orbit. For debris that can be cleared, ACOR optimization is used to obtain the clearing window corresponding to the shortest ablation time. The output of some of the debris is shown in Table 2. Debris no. 64, 234, and 370 can be effectively removed when the perigee is less than 200 km. Most of the debris-driven windows have conflicts, as shown in Figure 13.

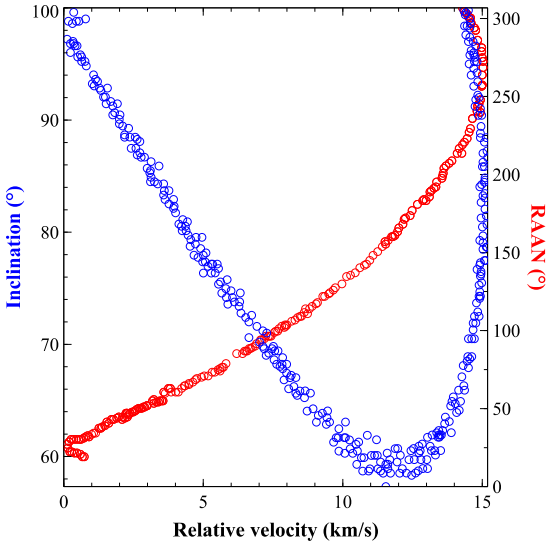

Figure 10. Distribution of relative velocity and orbital inclination/declination of ascending node.

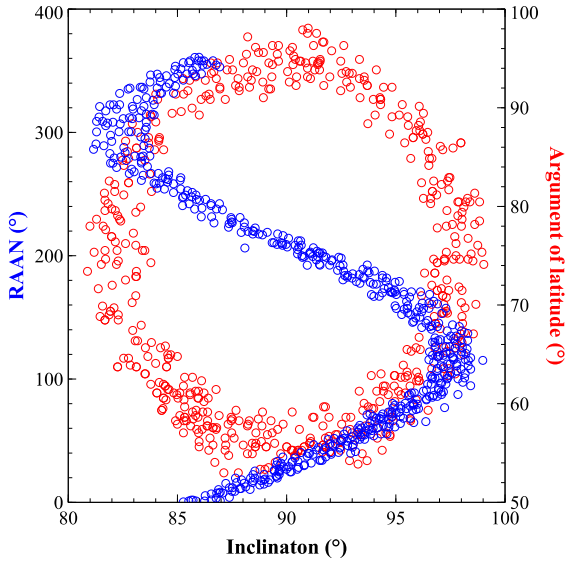

Figure 11. Distribution of declination/latitude argument and orbital inclination of ascending node.

Table 2. Results of single debris selection.

Debris No.	Start Point (s)	End Point (s)	Perigee before Ablation (km)	Perigee in the End (km)	Total Ablation Time (s)	Total Impulses (Counts)
5	3.366	9.1304	547.13	538.43	5.7644	577
9	0.4006	4.0593	646.80	644.98	3.6587	366
12	0.0025	1.0425	560.64	560.40	1.0400	104
13	0.1110	0.2911	551.62	540.51	0.1801	18
16	0.0559	1.0536	515.45	509.86	0.9977	100
20	0.0320	3.8829	485.59	482.39	3.8509	385
22	0.0198	2.6900	732.91	730.93	2.6702	267
23	2.4485	6.8648	578.77	333.93	4.4163	442
24	3.7218	64.6199	597.27	225.09	60.8981	6090
37	1.1161	24.2846	685.82	574.21	23.1685	2317
64	11.8880	104.4701	509.83	199.85	92.5821	9258
234	10.0590	167.2413	474.85	199.74	157.1823	15,718
370	24.1154	140.9113	520.92	199.78	116.7959	11,680

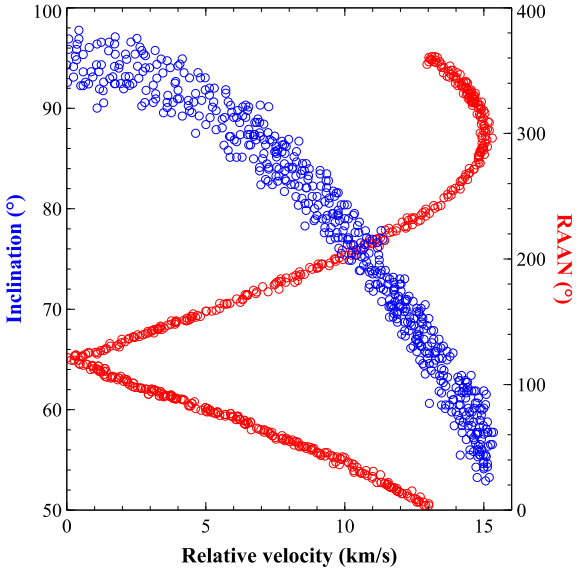

Figure 12. Distribution of relative velocity and orbital inclination/declination of ascending node.

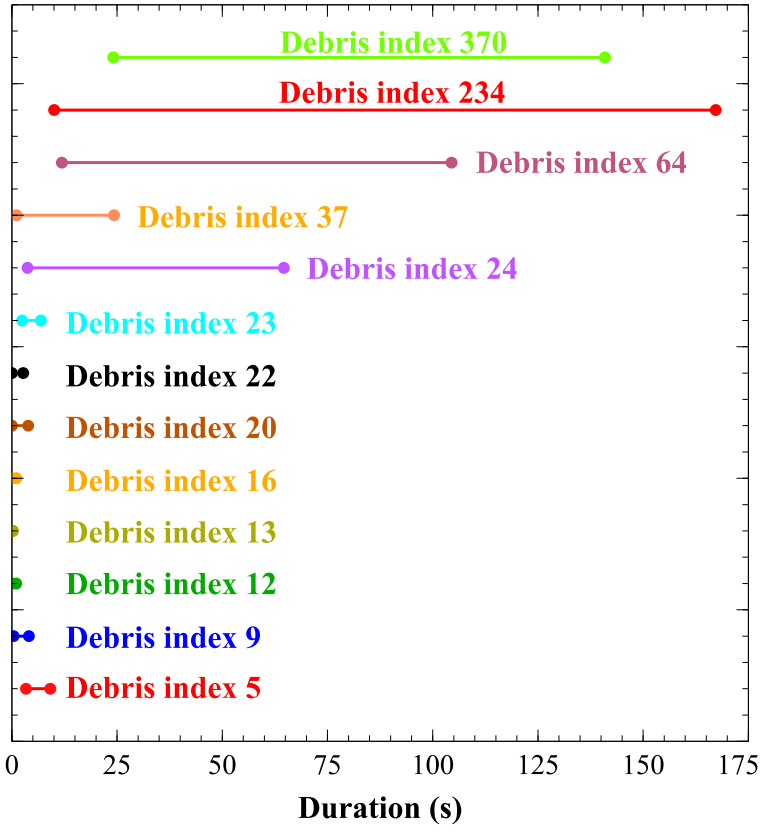

Figure 13. Ablation time window for some debris.

3.3. Multi Debris Selection

For 20 space debris with orbit reduction windows, the ant colony algorithm shown in Table 3 was used to obtain the optimal orbit reduction sequence as shown in Figure 14, and the optimization results are shown in Table 4. The driving sequence is 7-16-18-19. It can be seen that four debris were effectively lowered and two of them were successfully removed.

Table 3. Parameter settings for ant colony algorithm.

Parameters Name	Variable	Value
Number of ants	mAnt	20
Transfer Rule Parameters	str	0.5
Importance of pheromone	alpha	1
Importance of heuristic function	beta	3
Importance of waiting time	gama	1
Importance of window width for orbit reduction	delta	1
Pheromone volatilization factor	rho	0.85
Maximum number of iterations	iter_max	20
Stop condition for deviation of objective function	MaxStallGen	5

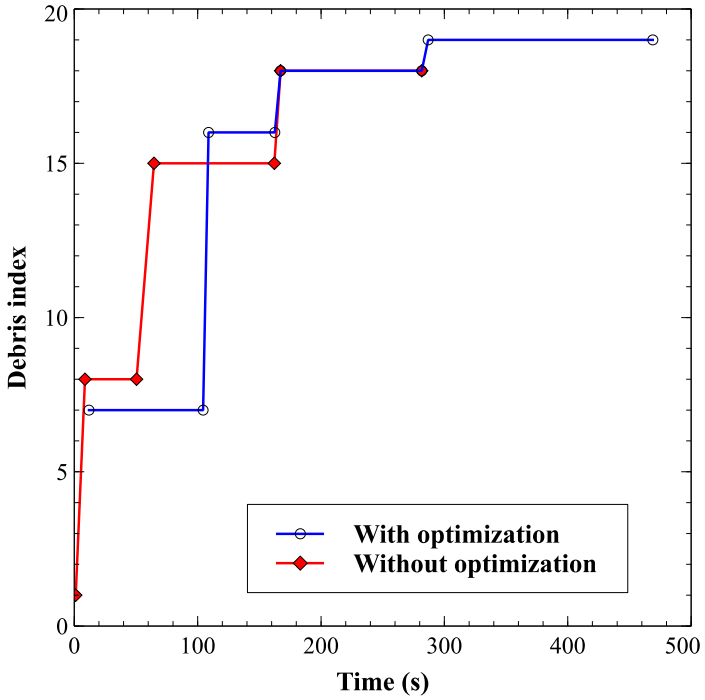

Figure 14. Ablation duration before and after optimization.

Table 4. Results of multiple debris selection with optimization.

Sequence No.	Debris No.	Start Point (s)	End Point (s)	Perigee before Ablation (km)	Perigee after Ablation (km)	Total Ablation Time (s)	Total Impulses (Counts)
7	64	11.8880	104.4701	509.8295	199.8850	92.5819	9259
16	269	108.8915	162.5621	595.7943	389.8226	53.6702	5367
18	234	167.2413	281.6858	474.8490	199.7381	114.4445	11,445
19	99	286.8095	468.8938	524.2445	450.2049	183.0840	18,309

If optimization is not entered, the regular driving sequence of the laser system is to sequentially drive the debris according to the entry time. It means continuously driving the first debris that enters the scope of the laser, and then moving on to the next debris when it leaves the scope o fthe laser or is effectively removed. The de-orbit effect obtained is shown in Table 5, with a driving sequence of 1-8-15-18. As shown in Figure 14, it can be seen that this scheme only effectively removes one debris from the orbit. From this, it is shown that after target selection and sequence optimization, the number of removable

debris has doubled, and the de-orbit effect has increased by 15.9%. The energy utilization rate of the laser system has increased by 74.6%.

Table 5. Results of multiple debris selection without optimization.

Sequence No.	Debris No.	Start Point (s)	End Point (s)	Perigee before Ablation (km)	Perigee after Ablation (km)	Total Ablation Time (s)	Total Impulses (Counts)
1	306	0.8238	1.1715	554.2266	553.2588	0.3476	34
8	351	8.6938	50.4794	556.0903	455.0806	41.7860	4179
15	24	64.6202	162.1677	597.2702	227.3991	97.5478	9755
18	234	167.2413	281.6858	474.8490	199.7381	114.4445	11,445

4. Conclusions

This study conducts research on the problem of target selection for a space-energy driven laser-ablation debris removal system based on ant colony optimization. Optimization algorithms for single target selection, optimal driving time windows, and multi-objective optimal driving sequences have been established. Calculation and verification have been conducted using the platform's peripheral debris information, produced by the Monte Carlo method, as samples. The results show that this algorithm can effectively meet the requirements of target selection and sequence optimization for the space-energy driven laser-ablation debris removal system. Compared with the situation without optimization, the number of removable debris is doubled, and the de-orbit effect is increased by 15.9%. The energy utilization rate of the space-energy driven laser-ablation debris removal system has increased by 74.6%. This algorithm is of great significance for the in-orbit engineering application of the space-energy driven laser-ablation debris removal system, especially for the process control of debris removal tasks of large-scale, high-energy, and high-frequency space-based pulse laser platforms.

In this paper, only ant colony optimization algorithms are used to study the screening and path planning of laser removal of space debris, but there are slow rates of convergence and local optimization problems. In the process of laser removal of space debris, there are various requirements such as maximizing the energy utilization rate of the removal system, optimizing the de-orbit effect, fast response ability, and orbital transfer, as well as removal scenarios under various distributions of space debris. In subsequent research, considering the initial state of debris and removal systems, hybrid and meta-acoustics algorithms could be used to study scenarios where a single removal system responds to multiple debris [39,40]. Considering the mutual cooperation and optimization among multiple systems, adaptive algorithms and self-adaptive algorithms could be used to study the scenario of removing space debris from a constellation composed of multiple removal systems [41,42]. Considering the characteristics of debris distribution intervals, island algorithms could be used to study the removal of multiple debris within different orbital ranges by relay [43,44]. In future research, the proposed approaches above could be effectively compared to each other to improve the efficiency of the last removal system.

Author Contributions: W.Y., H.F. and Z.S. designed the study and simulation; W.Y. and C.C. wrote the code; W.Y., Q.W. and C.C. conducted the data analysis; W.Y. and C.C. provided the mathematical methods; W.Y., Z.S. and C.C. drafted the paper; W.Y., H.F., Z.S., Q.W. and C.C. edited the paper. All authors have read and agreed to the published version of the manuscript.

Funding: This work was financially supported by the Special Fund for Space Debris Project (KJSP2020010304).

Institutional Review Board Statement: Not applicable.

Informed Consent Statement: Not applicable.

Data Availability Statement: Not applicable.

Acknowledgments: A special thanks is expressed to Zizheng Gong for his support with the simulation algorithm.

Conflicts of Interest: The authors declare no conflict of interest.

References

1. Alexander, L.; Vladimir, A. Review of contact and contactless active space debris removal approaches. *Prog. Aerosp. Sci.* **2022**, *134*, 100858.
2. Shan, M.; Shi, L. Comparison of Tethered Post-Capture System Models for Space Debris Removal. *Aerospace* **2022**, *9*, 33. [CrossRef]
3. Barea, A.; Urrutxua, H.; Cadarso, L. Large-scale object selection and trajectory planning for multi-target space debris removal missions. *Acta Astronaut.* **2020**, *170*, 289–301. [CrossRef]
4. Leomanni, M.; Bianchini, G.; Garulli, A.; Giannitrapani, A.; Quartullo, R. Orbit control techniques for space debris removal missions using electric propulsion. *J. Guid. Control. Dyn.* **2020**, *43*, 1259–1268. [CrossRef]
5. Phipps, C.R.; Boustie, M.; Chevalier, J.M.; Baton, S.; Brambrink, E.; Berthe, L.; Schneider, M.; Videau, L.; Boyer, S.A.R.; Scharring, S. Laser impulse coupling measurements at 400 fs and 80 ps using the LULI facility at 1057 nm wavelength. *J. Appl. Phys.* **2017**, *122*, 193103. [CrossRef]
6. Hakima, H.; Bazzocchi, M.C.F. Low-Thrust Trajectory Design for Controlled Deorbiting and Reentry of Space Debris. In Proceedings of the 2021 IEEE Aerospace Conference, Big Sky, MT, USA, 6–13 March 2021; Volume 50100, pp. 1–10.
7. Jankovic, M.; Yüksel, M.; Babr, M.M.; Letizia, F.; Braun, V. Space debris ontology for ADR capture methods selection. *Acta Astronaut.* **2020**, *173*, 56–68. [CrossRef]
8. Phipps, C.R.; Loktionov, E.Y.; Bonnal, C.; Boyer, S.A.E.; Sharaborova, E.; Tahan, G. Is laser space propulsion practical?: Review. *Appl. Opt.* **2021**, *60*, 1–11. [CrossRef]
9. Chang, H.; Ye, J.; Zhou, W. Effects of Typical Laser Wavelength on Impulse Coupling Characteristics Ablated by Nanosecond Pulsed Laser with Al Target. *J. Propuls. Technol.* **2015**, *36*, 1754–1760.
10. Stefan, S.; Jascha, W.; Eckel, H.A. Laser-based removal of irregularly shaped space debris. *Opt. Eng.* **2016**, *56*, 011007.
11. Phipps, C.R.; Luke, J.; Funk, D.; Moore, D.; Glownia, J.; Lippert, T. Laser impulse coupling at 130 fs. *Appl. Surf. Sci.* **2006**, *252*, 4838–4844. [CrossRef]
12. Mark, C.P.; Kamath, S. Review of Active Space Debris Removal Methods. *Space Policy* **2019**, *47*, 194–206. [CrossRef]
13. Jiang, T.; Cao, Y.F.; Ding, M. Progress of Space Debris Detection Technology. *Laser Optoelectron. Prog.* **2022**, *59*, 1415010.
14. Hakima, H.; Emami, M.R. Assessment of active methods for removal of LEO debris. *Acta Astronaut.* **2018**, *144*, 225–243. [CrossRef]
15. Scharring, S.; Eisert, L.; Lorbeer, R.A. Momentum predictability and heat accumulation in laser-based space debris removal. *Opt. Eng.* **2018**, *58*, 011004. [CrossRef]
16. Tsuno, K.; Wada, S.; Ogawa, T. Laser ablation induced impulse study for removal of space debris mission using small satellite. *Appl. Phys.* **2022**, *128*, 121–130. [CrossRef]
17. Zhao, S.; Steindorfer, M.; Kirchner, G. Attitude analysis of space debris using SLR and light curve data measured with single-photon detector. *Adv. Space Res.* **2020**, *65*, 1518–1527. [CrossRef]
18. Daisuke, S.; Yasuhiro, Y.; Toshiya, H.; Yuki, I.; Tadanori, F. Contactless attitude control of an uncooperative satellite by laser ablation. *Acta Astronaut.* **2022**, *196*, 275–281.
19. Sagnières, L.B.M.; Sharf, I.; Deleflie, F. Simulation of long-term rotational dynamics of large space debris: A TOPEX/Poseidon case study. *Adv. Space Res.* **2020**, *65*, 1182–1195. [CrossRef]
20. Ali, M. Interactive fuzzy Bayesian search algorithm: A new reinforced swarm intelligence tested on engineering and mathematical optimization problems. *Expert Syst. Appl.* **2022**, *187*, 115954.
21. Ali, M.; Mahsa, M. Differential evolution method integrated with a fuzzy decision-making mechanism and Virtual Mutant agent: Theory and application. *Appl. Soft Comput.* **2021**, *112*, 107808.
22. Ngoc, T.H.; Tien, V.T.N.; Nguyen, T.T.; Quoc-Manh, N. Optimizing Magnification Ratio for the Flexible Hinge Displacement Amplifier Mechanism Design. In Proceedings of the 2nd Annual International Conference on Material, Machines and Methods for Sustainable Development, Nha Trang, Vietnam, 12–15 November 2020; pp. 769–778.
23. Al-Nimr, M.; Milhem, A.; Al-Bishawi, B.; Al Khasawneh, K. Integrating Transparent and Conventional Solar Cells TSC/SC. *Sustainability* **2020**, *12*, 7483. [CrossRef]
24. Nazarenko, A.I.; Usovik, I.V. Space debris in low earth orbits region: Formation and reduction process analysis in past decade. *Acta Astronaut.* **2022**, *194*, 210231. [CrossRef]
25. Sarkar, M.; Barad, S.; Mohit, A. Development of a novel autonomous space debris collision avoidance system for uncrewed spacecraft. *Proc. Inst. Mech. Eng. Part G J. Aerosp. Eng.* **2022**, *236*, 2940–2952. [CrossRef]
26. Driedger, M.; Asgari, A.; Ferguson, P. Feasibility of Gathering Resident Space Object Range Measurements Using In-Orbit Observers. *IEEE J. Radio Freq. Identif.* **2022**, *6*, 250–257. [CrossRef]
27. Obukhov, V.A.; Kirillov, V.A.; Petukhov, V.G. Control of a service satellite during its mission on space debris removal from orbits with high inclination by implementation of an ion beam method. *Acta Astronaut.* **2022**, *194*, 390–400. [CrossRef]

28. Carvalho, J.; Moraes, R.D.; Prado, A. Analysis of the orbital evolution of space debris using a solar sail and natural forces. *Adv. Space Res.* **2022**, *70*, 125–143. [CrossRef]
29. Herrera-Jaramillo, D.A.; Henao-Bravo, E.E.; González Montoya, D.; Ramos-Paja, C.A.; Saavedra-Montes, A.J. Control-Oriented Model of Photovoltaic Systems Based on a Dual Active Bridge Converter. *Sustainability* **2021**, *13*, 7689. [CrossRef]
30. Miao, H.; Zhang, L.; Liu, S.; Zhang, S.; Memon, S.; Zhu, B. Laser Sealing for Vacuum Plate Glass with PbO-TiO_2-SiO_2-RxOy Solder. *Sustainability* **2020**, *12*, 3118. [CrossRef]
31. Tang, J.; Liu, G.; Pan, Q.T. A Review on Representative Swarm Intelligence Algorithms for Solving Optimization Problems: Applications and Trends. *IEEE/CAAJ* **2021**, *8*, 1627–1643. [CrossRef]
32. Jorgensen, M.K.; Sharf, I. Optimal planning for a multiple space debris removal mission using high-accuracy low-thrust transfers. *Acta Astronaut.* **2020**, *172*, 56–69. [CrossRef]
33. Viavattene, G.; Devereux, E.; Snelling, D.; Payne, N.; Wokes, S.; Ceriotti, M. Design of multiple space debris removal missions using machine learning. *Acta Astronaut.* **2022**, *193*, 277–286. [CrossRef]
34. Ajay, K.; Seema, B. Generalized Ant Colony Optimizer: Swarm-based meta-heuristic algorithm for cloud services execution. *Computing* **2019**, *101*, 1609–1632.
35. Liu, S.; Zhang, Q.; Zhou, D. Obstacle Avoidance Path Planning of Space Manipulator Based on Improved Artificial Potential Field Method. *J. Inst. Eng.* **2014**, *95*, 31–39. [CrossRef]
36. Zhang, T.; Shen, H.; Yang, Y. Ant Colony Optimization-based Design of Multiple-target Active Debris Removal Mission. *Trans. Jpn. Soc. Aeronaut. Space Sci.* **2018**, *61*, 201–210. [CrossRef]
37. Stuart, J.; Howell, K.; Wilson, R. Application of multi-agent coordination methods to the design of space debris mitigation tours. *Adv. Space Res.* **2016**, *57*, 1680–1697. [CrossRef]
38. Ntagiou, E.V.; Armellin, R.; Iacopino, C.; Policella, N.; Donati, A. Ant-based automated mission planning for data relay space missions. *J. Aerosp. Inf. Syst.* **2019**, *16*, 249–262. [CrossRef]
39. Zhao, H.T.; Zhang, C.S. An online-learning-based evolutionary many-objective algorithm. *Inf. Sci.* **2020**, *509*, 1–21. [CrossRef]
40. Maxim, A.D. An Adaptive Polyploid Memetic Algorithm for scheduling trucks at a cross-docking terminal. *Inf. Sci.* **2021**, *565*, 390–421.
41. Junayed, P.; Arriana, L.N.; Amir, M.; Tian, G.D.; Li, Z.W.; Wang, H.; Maxim, A.D. Exact and metaheuristic algorithms for the vehicle routing problem with a factory-in-a-box in multi-objective settings. *Adv. Eng. Inform.* **2022**, *52*, 101623.
42. Gholizadeh, H.; Fazlollahtabar, H.; Amir, M.F.F.; Maxim, A.D. Preventive maintenance for the flexible flowshop scheduling under uncertainty: A waste-to-energy system. *Environ. Sci. Pollut. Res.* **2021**, 1–20. [CrossRef]
43. Dulebenets, M.A.; Kavoosi, M.; Abioye, O.; Pasha, J. A Self-Adaptive Evolutionary Algorithm for the Berth Scheduling Problem: Towards Efficient Parameter Control. *Algorithms* **2018**, *11*, 100. [CrossRef]
44. Masoud, R.; Nastaran, O.A.; Niloofar, A.S. Ambulance routing in disaster response considering variable patient condition: NSGA-II and MOPSO algorithms. *J. Ind. Manag. Optim.* **2022**, *18*, 1035–1062.

Disclaimer/Publisher's Note: The statements, opinions and data contained in all publications are solely those of the individual author(s) and contributor(s) and not of MDPI and/or the editor(s). MDPI and/or the editor(s) disclaim responsibility for any injury to people or property resulting from any ideas, methods, instructions or products referred to in the content.